arXiv:1608.06653v2 [quant-ph] 21 Sep 2016

A characteristic function approach to the Jaynes-Cummings model revivals

Hudson Pimenta and Daniel F. V. James
Department of Physics, University of Toronto, 60 St. George Street, Toronto, Ontario M5S 1A7, Canada
(Dated: September 22, 2016)

A two-level atom interacting with an electromagnetic mode in a cavity experiences atomic inversion collapses and revivals. They are an indirect signature of the field quantization, and also hold information about the mode. Thus, they may be harnessed for quantum-state reconstruction. In this work, we study the revival structures with the characteristic function approach. The characteristic function is essentially a spectral decomposition of the photon-number probability distribution. Exploiting the characteristic function periodicity, we find that the inversion can be understood as the result of interference between a set of structures akin to a free quantum-mechanical wave packet, each structure corresponding to a snapshot of this packet for different degrees of dispersion. The packet Fourier representation determines the photon-number distribution of the electromagnetic mode. We then derive an integral equation whose solution yields the underlying packets. This approach allows the retrieval of the field photon-number distribution directly from the inversion under fairly general conditions, and paves the way for a new partial tomography technique.

I. INTRODUCTION

Experiments in quantum optics have by now unequivocally established the granular and quantum nature of the electromagnetic field [1–4]. Technology has since improved to the point that many sorts of quantum states of the field can be synthesized [5–9]. They can also be studied in much more controllable environments, such as cavities, giving rise to a field called cavity electrodynamics (cavity QED) [10–13]. In a typical cavity experiment, an atom traverses a cavity and interacts with an electromagnetic field mode. Understanding the dynamics of this interaction enables further probing of the predictions of quantum mechanics and its exploitation for various applications [14–16].

In the context of cavity QED, an important model is the Rabi model [17, 18], which describes a single electromagnetic mode coupled to a two-level atom. Though it can be solved exactly [19], this model affords a much simpler picture when the field-atom coupling is weak. Then the model may be approximated by the paradigmatic Jaynes-Cummings model (JCM) [20, 21]. Despite its simplicity, the JCM has remarkable features associated with the granular nature of photons. Some of the most striking of these features are the atomic inversion collapses and revivals [21, 22].

The collapses and revivals are a result of interference between inversion oscillations with different frequencies, each corresponding to a possible number of photons n inside the cavity. The revivals, in particular, are only possible because the number of photons is discrete. Therefore, they are an indirect signature of the EM field quantization. Moreover, the revivals quasi-periodicity provides evidence for the JCM anharmonic energy ladder (which has been observed through population measurements [23] and, more directly, through spectroscopy [24]). Inversion revivals have been extensively investigated in the literature [22, 25–30].

Besides their historical relevance, the revivals also hold potential for characterizing the field state, since the inversion profile is directly dictated by the field photon-number amplitudes. Determining the field quantum state from experimental data is the aim of quantum-state reconstruction [31, 32]. In the more traditional approach, we represent a quantum state by a density matrix, the elements of which are to be determined by repeated measurements of a set of observables [33]. For example, in the context of a two-level system, these observables may be the ones associated to the Pauli matrices [34].

A mode of the electromagnetic field, however, is more complicated. Firstly, since it is a quantum harmonic oscillator, there are infinitely many matrix elements to be determined. Moreover, when its density operator is represented in the basis of Fock states, population measurements require photon-number resolving techniques, which have become available only much more recently [35, 36].

For this reason, historically, tomography for the field took a different path, by exploring representations of the state in terms of phase space quasi-probability distributions [37, 38]. One of the most popular distributions is the Wigner function [39]. It contains information about the generalized field quadrature probability distributions [31]. By measuring these distributions through balanced homodyne detection, it is possible to reconstruct the Wigner function [40–42]. Later proposals use the same data to obtain the density matrix directly [43, 44]. Unbalanced homodyning is also a possibility [45, 46].

Yet another tomographic approach consists of coupling the field to an auxiliary simpler system from which information about the field is retrieved indirectly. It is in this context that cavity QED and the JCM revivals insert. It has been shown that, when an inversion revival may be isolated, it may be used to retrieve photon-number distributions [47]. A phase-sensitive scheme that uses population curves for different atomic coherent superpositions for reconstruction has also been proposed [48]. An alternative that avoids the coherent superposition technicalities consists of displacing the field state instead [49]. Moreover, atomic population measurements may also be

used to probe the Wigner function [50].

With the goal of investigating alternative approaches for quantum harmonic oscillators tomography, we investigate the Jaynes-Cummings inversion via the approach of the field mode distribution characteristic function [51]. Characteristic functions are the Fourier representation of a distribution. In this paper, we use their properties to decompose the inversion into into much simpler, localized in time, packets, with shape dictated by the photon-number characteristic function. We show that each packet is akin to a snapshot of a free quantum-mechanical wave-packet at a different effective time. Hence, just as in quantum mechanics, knowledge of a single packet is enough to generate every other packet and, therefore, the whole inversion.

The advantages of this approach are as follows. Firstly, it shows that the inversion contains highly redundant information (besides being an awkward function for analytical and numerical manipulations due to its slowly-decreasing behaviour). By contrast, a single one of the packets we introduce in this work contains the complete physics of the inversion. We also argue that, when they do not overlap, each may be identified with a single revival, in which case the photon-number distribution may be retrieved immediately [47].

Secondly, even when revivals cannot be resolved, the underlying picture of a superposition of packet persists. It is then that the snapshot decomposition is the most advantageous: we use it in this work cast aside the limitation of non-overlapping revivals, and retrieve the photon-number distribution under much more general conditions. The key idea is that the snapshot to be retrieved is usually concealed behind an overly complex inversion profile. However, within a properly chosen time window, this inversion is simply this snapshot, albeit contaminated by tails of adjacent snapshots.

If different snapshots were all unrelated, this would spell doom for any attempts at its retrieval. However, due to the quantum-mechanical analogy, a sum of different snapshots may be ultimately reduced to an integral equation involving just a single one of them. Solving this equation yields the packet with full information about the inversion and, therefore, the photon-number distribution. In this work, we illustrate our approach mostly through coherent states due to their simplicity. However, we emphasize the generality of this method, which will be explored more meticulously, and for a larger variety of states, in a future work. The present work lays the groundwork for this new form of partial tomography.

This paper is organized as follows. Sec. II reviews the JCM and its population quasi-periodic revivals. We also introduce periodic revivals, due to their simplicity and also because many of their qualitative features persist in the quasi-periodic case. Sec. III considers the periodic and quasi-periodic revivals in terms of the characteristic function. We use its properties to split the revivals and reveal the packets underlying the inversion for a field in a general state. We consider a coherent state as an example, but reiterate that generality of this decomposition. Sec. IV exemplifies the formalism previously developed for a cat state. Finally, Sec. V highlights the novelty of this approach by discussing the extraction the packets and the photon-distribution for a very general inversion profile. Finally, Sec. VI summarizes our results.

II. COLLAPSES AND REVIVALS

In this section, we review the collapses and revivals in the JCM. The JCM descends from the Rabi model, which describes a single electromagnetic mode coupled to a single two-level atom [17, 18]. The Rabi Hamiltonian reads ($\hbar = 1$)

$$\hat{H}_R = \omega \hat{a}^\dagger \hat{a} + \frac{\omega_0}{2}\hat{\sigma}_z + g\hat{\sigma}_x(\hat{a}^\dagger + \hat{a}), \tag{1}$$

where $\hat{a}$ is the annihilation operator for a photon in an electromagnetic mode of frequency ω, ω_0 is the splitting between the two atomic levels and g is field-atom coupling constant. The two-level atom has been mapped into a pseudospin $\hat{\sigma}$, with ground state $|g\rangle$ and excited state $|e\rangle$ corresponding to spin down and up in the z-direction, respectively. In this language, $\hat{\sigma}_x = \hat{\sigma}_+ + \hat{\sigma}_-$ represents the atomic dipole moment. Assuming weak field-atom coupling, i. e., $g \ll \omega,\ \omega_0$, we neglect terms in the Hamiltonian proportional to $\hat{a}\hat{\sigma}_-$ and $\hat{a}^\dagger\hat{\sigma}_+$. They lead to costly energy transitions ($\sim \omega + \omega_0$) when compared to those generated by $a\sigma_+$ and $a^\dagger\sigma_-$ ($\sim \omega - \omega_0$). This leads to

$$\hat{H}_{JC} = \omega \hat{a}^\dagger \hat{a} + \frac{\omega_0}{2}\hat{\sigma}_z + g(\hat{a}^\dagger\hat{\sigma}_- + \hat{a}\hat{\sigma}_+), \tag{2}$$

which is known as the JCM Hamiltonian.

In this small g limit, an atom transitioning away from the excited state (ground state) is always followed by a photon emission (absorption). Hence, the state of the system initially given by $|e, n\rangle$, where $|n\rangle$ is the Fock state with n photons, will oscillate between $|e, n\rangle$ and $|g, n+1\rangle$ as

$$\begin{aligned}\hat{U}(t)|e, n\rangle = &\cos\left(\frac{\Omega_n}{2}t\right)|e, n\rangle \\ &+ i\sin\left(\frac{\Omega_n}{2}t\right)|g, n+1\rangle,\end{aligned} \tag{3}$$

where $\Omega_n = 2g\sqrt{n+1}$.

The atomic populations in the ground and excited states are then $P_g(t) = \sin^2\left(\frac{\Omega_n}{2}t\right)$ and $P_e(t) = \cos^2\left(\frac{\Omega_n}{2}t\right)$, respectively. It is customary to define the population inversion as the difference between these populations: $W(t) \equiv P_e(t) - P_g(t)$. For $|e, n\rangle$ as initial state, inversion is simply $\cos(2g\sqrt{n+1}t)$. However, more generally, the field state is a superposition of Fock states $|n\rangle$ with different photon-number amplitudes c_n. Assuming

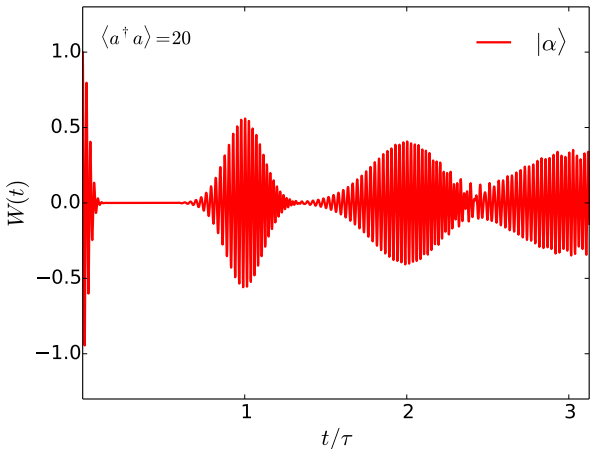

Figure 1. Atomic inversion of Eq. (4) as a function of time. The atom is initially excited and the field is in a coherent state with average photon-number of 20. Time is measured in units of τ, where τ is the time for which the first revival amplitude is maximum. The dephasing of the oscillators in Eq. (4) lead to inversion collapses. With discrete yet incommensurable frequencies, the inversion has revivals, but they are only quasi-periodic. The revival peaks are approximately equally spaced by τ.

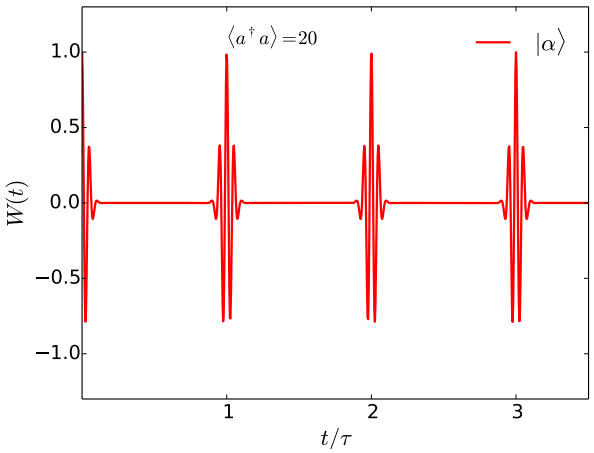

Figure 2. Inversion as a function of time when the frequencies are commensurable, as in Eq. (5). The atom is initially excited and the field is in a coherent state with average photon-number of 20. Time is measured in units of τ, where $\tau = \pi$ is the inversion period. With only commensurable frequencies, the inversion is exactly periodic.

that atom is still initially excited, the inversion takes the more general form

$$W(t) = \sum_{n=0}^{+\infty} |c_n|^2 \cos\left(2g\sqrt{n+1}t\right), \tag{4}$$

where $|c_n|^2 \equiv P_n$ is the field photon-number distribution.

A great deal of attention has been given to the inversion because it provides evidence of the electromagnetic field quantization through its collapses and revivals [21]. We illustrate the inversion for a coherent state in Fig. 1. For short times, $W(t)$ is dominated by Rabi-like oscillations. As the oscillators of Eq. (4) dephase, they interfere destructively, causing the collapse. Still, the discreteness of the frequencies, a direct consequence of the field quantization, allows for population revivals at later times. The revivals are not, however, periodic, since some frequencies are incommensurable, i. e., their ratios are irrational numbers.

The inversion $W(t)$ is interesting also because it holds information about the field photon-number distribution P_n. However, the incommensurable frequencies hampers the distribution retrieval: Eq. (4) looks like a Fourier series, but it is not, due to the frequencies incommensurability. An inversion formula is known when a single revival of $W(t)$ can be isolated [47].

To support the next section discussion, we also present (exactly) periodic revivals. They may be seen as mathematical constructs defined by the replacement $\sqrt{n+1} \to n$ in Eq. (4):

$$W_p(t) = \sum_{n=0}^{+\infty} |c_n|^2 \cos\left(2gnt\right). \tag{5}$$

The lower index p is a reminder that this inversion is not the same as the JCM inversion. The frequencies in Eq. (5) are all commensurable. Hence $W_p(t)$ is exactly periodic, the period given by $T = \pi/g$. Unlike Eq. (4), Eq. (5) is an actual Fourier series, and may be inverted immediately. We illustrate the periodic revivals in Fig. 2 under the same conditions of Fig. 1. The periodic revivals are very useful for interpreting the JCM revivals, since both share many qualitative features. For instance, in both Figs. 1 and 2, the revival peaks seem to be periodically spaced.

As a side note, there are models for which Eq. (5) in fact describes the atomic population dynamics [52–54]. For example, Knight proposed a system where the levels $|g\rangle$ and $|e\rangle$ are degenerate and connected by two-photon transitions through a higher-energy virtual level [53]. The Hamiltonian describing this process is

$$\hat{H} = \omega\hat{a}^\dagger\hat{a} + g\hat{a}^\dagger\hat{a}\hat{\sigma}_x. \tag{6}$$

With an initially excited atom, the inversion for this model is precisely $W_p(t)$.

To set the scene for the next section, we introduce the auxiliary function

$$Z(t) = \sum_{n=0}^{+\infty} P_n e^{i2\pi f(n)t}, \tag{7}$$

which is the complex extension of both Eqs. (4) and (5). Setting $f(n)$ to $g\sqrt{n+1}/\pi$ or gn/π and taking the real

part of $Z(t)$ yields $W(t)$ or $W_p(t)$, respectively. From now on, we will simply write $f(n) \propto n$ or $f(n) \propto \sqrt{n+1}$. For simplicity, most of our computations are done with $Z(t)$.

While periodic revivals are very straightforward to understand, quasi-periodic revivals have resisted a simple picture. Approximation schemes have been developed for specific photon-number distributions [22], but the incommensurable frequencies make Eq. (4) quite difficult to treat in general. On the other hand, the simplicity of periodic revivals lies in that knowledge of a single revival cycle is enough to generate the inversion for any time.

The striking result we show in the next section is that a similar picture actually holds true for the JCM quasi-periodic revivals: the inversion is composed of underlying packets. The packets are not perfect replicas of one another, but knowing just one of them suffices to determines the inversion completely. However, unlike the whole inversion, the packets are usually localized in time, which makes them more more useful for practical applications. We prove these claims in the next section by introducing characteristic functions.

III. DECOMPOSING THE INVERSION WITH THE CHARACTERISTIC FUNCTION

In Sec. II, we briefly reviewed the JCM, its inversion quasi-periodic revivals, and some corresponding periodic revivals. We introduced the auxiliary function $Z(t)$ in Eq. (7) to contemplate both kinds of revivals simultaneously. When $f(n) \propto n$ or $f(n) \propto \sqrt{n+1}$, the real part of $Z(t)$ yields $W(t)$ or $W_p(t)$, respectively. In this section, we investigate $Z(t)$ further using characteristic functions.

The characteristic function of a probability distribution P_n is defined as the expectation value of $e^{i2\pi kn}$ [51], i. e.,

$$\chi(k) \equiv \sum_{n=0}^{+\infty} P_n e^{i2\pi kn}. \tag{8}$$

The function $\chi(k)$ is also simply a Fourier series with P_n as coefficients. It contains just as much physical information as P_n, which is obtainable from $\chi(k)$ by inverting Eq. (8):

$$P_n = \int_{-\frac{1}{2}}^{\frac{1}{2}} dk\ \chi(k) e^{-i2\pi kn}. \tag{9}$$

Due to P_n being a discrete distribution, its characteristic function, just like $W_p(t)$ in Eq. (4), is a periodic function: $\chi\left(k - \frac{1}{2}\right) = \chi\left(k + \frac{1}{2}\right)$.

It is not a mere coincidence that $\chi(k)$ and $W_p(t)$ are both periodic: with the identification $k = \frac{gt}{\pi}$, $W_p(t)$ is the real part of $\chi(k)$. This follows from realizing that, when $f(n) \propto n$, the inversion complex extension $Z(t)$ is the characteristic function itself: $Z(t) = \chi(gt/\pi)$.

When $f(n) \propto \sqrt{n+1}$, the connection between $\chi(k)$ and $Z(t)$ is not so immediate. That said, we have seen in Fig. 1 that the quasi-periodic revivals, to some extent, have equally spaced peaks. This suggests that, even after replacing commensurable frequencies by incommensurable ones, $Z(t)$ seems to still inherit some properties of $\chi(k)$, such as its periodicity, to a certain degree. Our goal is to put this connection on more precise grounds by expressing $Z(t)$ in terms of $\chi(k)$ for a general $f(n)$.

With this goal in mind, we introduce the distribution

$$P(x) \equiv \sum_{n=0}^{+\infty} P_n \delta(x - n) \tag{10}$$

which allows us to rewrite rewrite $Z(t)$ as

$$Z(t) = \int_{-\infty}^{+\infty} dx P(x) e^{i2\pi f(x)t}, \tag{11}$$

where $f(x)$ is just the extension of $f(n)$ to real numbers, e. g., $n \to x$ and $\sqrt{n+1} \to \sqrt{x+1}$. It is easy to check from Eq. (8) that the distribution $P(x)$ also has $\chi(k)$ as its characteristic function:

$$P(x) = \int_{-\infty}^{+\infty} dk\ \chi(k) e^{-i2\pi kx}. \tag{12}$$

Unlike Eq. (9), the integral in Eq. (12) is not bounded, which will be useful in the next steps.

We now substitute from Eq. (12) into Eq. (11) to express $Z(t)$ in terms of $\chi(k)$:

$$Z(t) = \int_{-\infty}^{+\infty} dk\ \chi(k) \int_{-\infty}^{+\infty} dx\ e^{i2\pi[f(x)t - kx]}. \tag{13}$$

The integral over x is some distribution dependent on k and t, which we will denote $\mathcal{K}(k,t)$:

$$\mathcal{K}(k,t) \equiv \int_{-\infty}^{+\infty} dx\ e^{i2\pi[f(x)t - kx]}. \tag{14}$$

It may be interpreted as a propagator that determines $Z(t)$, given $\chi(k)$. Unlike $\chi(k)$, the propagator is not necessarily periodic with respect to k. This ultimately leads to $Z(t)$ not being exactly periodic in general.

Next, we use the periodicity of $\chi(k)$ to split the integral over k in Eq. (13) into a sum of integrals, each of which ranging from $m - \frac{1}{2}$ to $m + \frac{1}{2}$, with $m \in \mathbb{Z}$. Then, for each interval, we make the change of variables $k \to k+m$, so that each integral covers the same range $[-1/2, 1/2)$. Eq. (13) then simplifies to

$$Z(t) = \sum_{m=-\infty}^{+\infty} Z_m(t), \tag{15}$$

$$Z_m(t) = \int_{-\frac{1}{2}}^{\frac{1}{2}} dk\ \chi(k) \mathcal{K}(k+m, t), \tag{16}$$

where the periodicity of $\chi(k)$ allows us to replace $\chi(k+m)$ by $\chi(k)$.

The decomposition in Eq. (15) involves no approximation. We now specialize Eq. (16) for the cases $f(n) \propto n$ and $f(n) \propto \sqrt{n+1}$. We show that, in both cases, knowledge of a single $Z_m(t)$ is enough to determine $Z(t)$.

A. The case $f(n) \propto n$

When $f(n) \propto n$, it is easy to verify that $\mathcal{K}(k+m,t)$ is simply $\delta\left(k+m-\frac{gt}{\pi}\right)$. Since k only ranges from $-1/2$ to $1/2$ in Eq. (16), gt/π must be in the range of $m-1/2$ and $m+1/2$ for $\delta\left(k+m-\frac{gt}{\pi}\right)$ to contribute. Therefore, for a given t, only a single $Z_m(t)$ is not zero, and happens to be the characteristic function when we use the delta function to integrate:

$$Z_m(t) = \chi\left(\frac{gt}{\pi}\right)\Pi\left(\frac{gt}{\pi}-m\right), \tag{17}$$

where $\Pi(x)$ is the rectangular function, equal to 1 for $-1/2 < x < 1/2$ and 0 otherwise.

Hence, each $Z_m(t)$ is a replica of every other one, centered at $gt_m = m\pi$. In Fig. 2, each revival corresponds to the real part of a different $Z_m(t)$. We show next that, for $f(n) \propto \sqrt{n+1}$, a similar picture also holds true, except that the $Z_m(t)$ are not perfect copies of one another: they also experience dispersion akin to that of quantum-mechanical wave packets.

B. The case $f(n) \propto \sqrt{n+1}$

When $f(n) \propto \sqrt{n+1}$, the propagator $\mathcal{K}(k,t)$ is more complicated, but the decomposition of $Z(t)$ as a sum of $Z_m(t)$ remains exact. The non-periodicity of $\mathcal{K}(k,t)$ implies that $Z_m(t)$ now actually depends on m. Also, since $\mathcal{K}(k,t)$ is not a delta function, the simple identification $k = gt/\pi$ found for the case $f(n) \propto n$ does not hold.

In spite of such complications, as we continuously deform $f(n)$ from n to $\sqrt{n+1}$, we expect periodic revivals such as the ones in Fig. 2 to gradually yield place to the quasi-periodic revivals such as the ones in Fig. 1. If these revivals do not overlap during the process, it is natural to associate each JCM revival to a single $Z_m(t)$. In this scenario, the first collapse, in particular, would be identified with

$$Z_0(t) = \int_{-1/2}^{1/2} dk\ \chi(k) \int_{-\infty}^{\infty} dx\ e^{i2\pi[f(x)t-kx]}. \tag{18}$$

A technical detail worth mentioning is that the definition of $Z_0(t)$ must encompass a portion of the region $t<0$. This is easier to justify through periodic revivals. In Fig. 2, we see that the region near $t=0$ only comprehends half of the structure replicated at later times, so we must extend $Z(t)$ for $t<0$ to capture the missing half. This must, then, also be true for quasi-periodic revivals. On the other hand, in an experimental setup, one may measure only $W(t) = \Re\{Z(t)\}$, and only for $t>0$. However, since $W(t)$ is an even function, it can be readily extended to $t<0$.

We now show that a single $Z_m(t)$ has complete information about the whole $Z(t)$. This is more easily seen in Fourier space, where it will be clear that the Fourier transform of each $Z_m(t)$ differs only by a phase from every other one. We define the Fourier transform of $Z_m(t)$ as

$$\tilde{Z}_m(\nu) \equiv \int_{-\infty}^{+\infty} dt\ e^{i2\pi\nu t} Z_m(t). \tag{19}$$

Then, Fourier-transforming both sides of Eq. (16), it follows that

$$\tilde{Z}_m(\nu) = \int_{-1/2}^{1/2} dk\ \chi(k) \int_{-\infty}^{\infty} dx\ \delta\left[f(x)-\nu\right] e^{-i2\pi(k+m)x}, \tag{20}$$

The integral over x can be readily performed by using the property $\delta\left[g(x)\right] = \sum_i \frac{\delta(x-x_i)}{g'(x_i)}$, where x_i are the roots of $g(x)$. For $f(x) = g\sqrt{x+1}/\pi$, we have a single root, $x = \left(\frac{\pi\nu}{g}\right)^2 - 1$, and only if $\nu > 0$. If $\nu < 0$, there is no solution, which implies that $\tilde{Z}_m(\nu) = 0$ for $\nu < 0$. This also follows from $Z(t)$ being a sum of only positive frequencies signals, according to Eq. (7).

Finally, after integrating the right-hand side of Eq. (20) over x and moving every factor independent of k to the left-hand side, we get

$$\left(\frac{g}{2\pi}\right)^2 \frac{\tilde{Z}_m(\nu)}{\nu} e^{i2\pi m\left(\frac{\pi\nu}{g}\right)^2} = \begin{cases} \displaystyle\int_{-1/2}^{1/2} dk\ \chi(k) e^{-i2\pi k\left[\left(\frac{\pi\nu}{g}\right)^2-1\right]}, & \text{if } \nu > 0; \\ 0, \quad \text{otherwise.} \end{cases} \tag{21}$$

Intriguingly, only the left-hand side of Eq. (21) depends on m. This means that each $\tilde{Z}_m(\nu)$ can differ only by a phase from one another:

$$\tilde{Z}_m(\nu) = \tilde{Z}_0(\nu) e^{-i2\pi m\left(\frac{\pi\nu}{g}\right)^2}. \tag{22}$$

This relation is one of the major results of this work, and we now discuss its implications. The phase we just encountered depends on ν quadratically. If the dependence were linear, this phase would simply translate $Z_0(t)$ in time. However, it is well-known from quantum dynamics of free particles that quadratic dependencies lead to an overall translation, but also to some dispersion.

To make this analogy clearer, consider a quantum-mechanical wave packet in free space $\psi(x)$, and its Fourier transform $\tilde{\psi}(p)$, describing a particle of mass $\mu = 1/2$. The time-evolved $\psi(x,\tau)$ is obtained by taking

the inverse Fourier transform of $\tilde{\psi}(p)e^{-i\tau p^2}$. The analogy goes as follows: x, $\psi(x)$, p and $\tilde{\psi}(p)$ correspond to t, $Z_0(t)$, ν and $\tilde{Z}_0(\nu)$, respectively; and $Z_m(t)$ corresponds to $\psi(x,\tau)$, with m determining the effective τ.

In quantum mechanics, a packet propagates over space and disperses as it moves. Each $Z_m(t)$ is analogous to a snapshot of the wave packet. The inversion is the superposition of the snapshots. Nonetheless, a single snapshot $Z_m(t)$ is enough to determine every other snapshot, just as knowledge of the quantum-mechanical wave packet for some instant implies knowledge of it for any other instant. Hence, a single $Z_m(t)$ determines the inversion completely.

Therefore, while $Z(t)$ and $W(t)$ may, in general, look very irregular and complicated, it should be possible to distill them and identify an underlying pattern corresponding to the juxtaposition of different $Z_m(t)$ or $W_m(t) \equiv \Re\{Z_m(t)\}$. Next, we illustrate the distillation for a coherent state with average photon-number of 20. The first step is to identify $Z_0(t)$. We already argued that, if the collapse and the first revival do not overlap, we may associate $Z_0(t)$ with the collapse. We then numerically compute $\tilde{Z}_0(\nu)$ through the Fast Fourier Transform (FFT) method [55]. With Eq. (22), we find the subsequent $\tilde{Z}_m(\nu)$. Finally, the inverse FFT of $\tilde{Z}_m(\nu)$ yields $Z_m(t)$.

We present the results of this procedure in Fig. 3, where we have considered $m = 0, 1, 2, 3, 4$. In Fig. 3 (a), we simply juxtapose (the real part of) each $Z_m(t)$. In Fig. 3 (b), we add them up. Here, the blue curve corresponds to $\sum_{m=0}^{4} W_m(t)$ and the red curve (visible only after $gt \sim 110$) is the actual $W(t)$, calculated numerically with Eq. (4). The agreement can be improved for longer times by adding more $W_m(t)$.

Following the analogy with quantum mechanics, we estimate at what time each $Z_m(t)$ is centered. Whereas in quantum mechanics one linearizes the dispersion relation, here we linearize the phase in Eq. (22) around some frequency $\tilde{\nu}$ at which $\tilde{Z}_0(\nu)$ is peaked. With $Z_0(t)$ centered at 0, $Z_m(t)$ should be centered at

$$t_m = 2m\left(\frac{\pi}{g}\right)^2 \tilde{\nu}. \tag{23}$$

There must correspond a photon number to the dominant frequency $\tilde{\nu}$, which we define through $2\pi\tilde{\nu} \equiv 2g\sqrt{\tilde{n}+1}$. In terms of $\tilde{n}$,

$$t_m = \frac{2\pi\sqrt{\tilde{n}+1}}{g} m, \tag{24}$$

Naturally, these times also correspond to when the terms of Eq. (4) are approximately in phase [56]. In a loose sense, $\tau \equiv \dfrac{2\pi\sqrt{\tilde{n}+1}}{g}$ works as a period, except that $Z_m(t)$ also widens as we increase m. This explains why

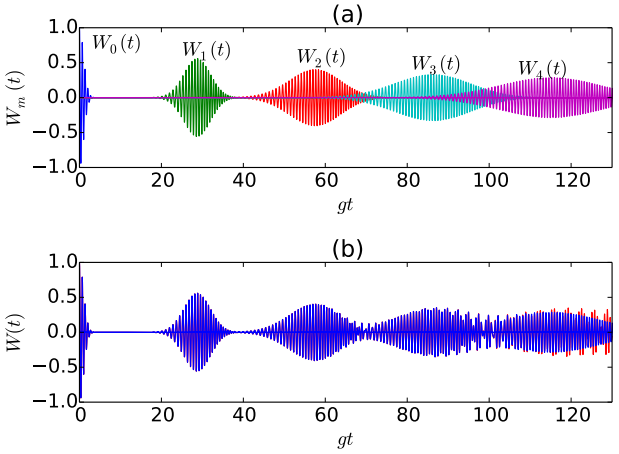

Figure 3. We consider the revivals for a coherent state with average photon-number of 20 in light of the decomposition of Eq. (15). In Fig. 3 (a), we juxtapose different $W_m(t)$. According to Eq. (22), they become the same once dispersion is accounted for. The kind of dispersion is the same experienced by free wave packets in quantum mechanics. In Fig. 3 (a), we compare the result of adding these replicas (blue curve) and the actual population inversion (red curve). There is excellent agreement, except for longer times ($gt \sim 110$), which may be fixed by adding subsequent $W_m(t)$.

the revival peaks in Fig. 1 are approximately equally spaced. Since the $Z_m(t)$ are ultimately are generated by $\chi(k)$, it is natural to make the more general identification

$$t \to \frac{2\pi\sqrt{\tilde{n}+1}}{g} k, \tag{25}$$

so that, when we increment k by one, t also changes by τ.

To finish this section, we discuss how to obtain the probabilities from a single $Z_m(t)$, a relevant task in the context of quantum tomography. Firstly, we notice that the right-hand sides of Eqs. (21) and (9) have very similar forms. It follows that, by setting $\nu = \nu_n$, where $2\pi\nu_n \equiv 2g\sqrt{n+1}$, the right-hand side of Eq. (21) becomes simply P_n. On the left-hand side of Eq. (21), replacing ν by ν_n eliminates the phase factor. We are then left simply with

$$P_n = \frac{g^2}{2\pi^2}\frac{\tilde{Z}_m(\nu_n)}{\nu_n}. \tag{26}$$

Notice that $2\pi\nu_n = 2g\sqrt{n+1}$ are the oscillation frequencies of the oscillators in Eq. (4).

It is interesting to rewrite Eq. (26) in terms of the actually measurable $W(t)$. Firstly, we define $W_m(t) = \Re\{Z_m(t)\}$, and $\tilde{W}_m(\nu)$ as its Fourier transform. Then it is not hard to show that $\tilde{W}_m(\nu) = \dfrac{\tilde{Z}_m(\nu)}{2}$ for $\nu > 0$. Therefore,

$$P_n = \frac{g^2}{\pi^2}\frac{\tilde{W}_m(\nu_n)}{\nu_n}. \tag{27}$$

A similar relation was previously obtained through a Poisson sum formula approach under the assumption of non-overlapping revivals [47]. Eq. (27) states that the probability distribution is codified in the frequencies of $W_m(t)$ present in Eq. (4).

Nevertheless, the relation between probabilities and $W_m(t)$ is exact, since it follows from Eqs. (15) and (16). However, experimentally, only the whole $W(t)$ can be measured. Thus, having non-overlapping revivals is more of a convenience, as it allows us to approximately identify the m-th revival of $W(t)$ to $W_m(t)$ immediately. In this regime, our method is equivalent to that Ref.[47]. However, particularly for low average photon-numbers, this approximation breaks down already for $m = 0$. It is then that our formalism shines: we use it in Sec. V to cast away this limitation and retrieve $W_0(t)$ even when revivals overlap.

We now use $W_0(t)$ and $W_1(t)$, previously shown in Fig. 3, to retrieve the photon-number distribution of a coherent state with $\langle a^\dagger a\rangle = 20$. The results are shown in Fig. 4. The red circle-shaped dots are the theoretical P_n. The dashed curves are the right-hand side of Eqs. (27) for $m = 0$ and $m = 1$. We convert the argument ν to n through the identification $2\pi\nu = 2g\sqrt{n+1}$. Eq. (27) predicts that, when n is an integer, the plotted function should match P_n, which is consistent with the behaviour of the dashed curves. Moreover, the faster-oscillating purple line, which corresponds to $m = 1$, has the blue line ($m = 0$) as its envelope, in agreement with Eq. (22).

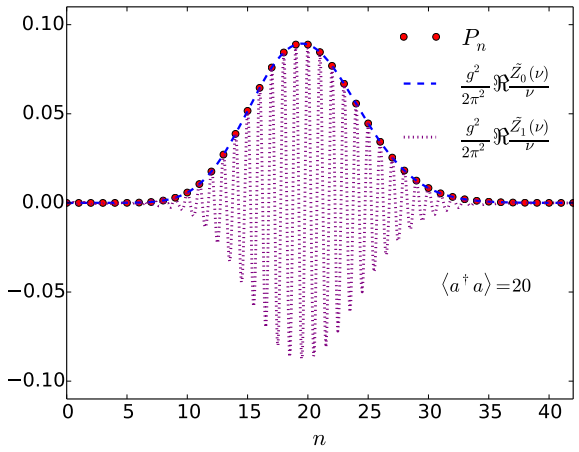

Figure 4. Comparison between the photon-number distribution P_n of a coherent state with average photon-number of 20 and the functions $\frac{g^2}{\pi^2}\frac{\tilde{W}_m(\nu)}{\nu} = \frac{g^2}{2\pi^2}\frac{\Re\{\tilde{Z}_m(\nu)\}}{\nu}, m = 0, 1$, showing the validity of Eq. (27). It is also worth mentioning that the function with $m = 1$ is enveloped by the one with $m = 0$, in agreement with Eq. (22).

IV. DISTILLING THE REVIVALS OF A CAT STATE

In the previous section, we have shown that the JCM population revivals are a result of interference between a set of packets $Z_m(t)$, which are akin to snapshots of a quantum-mechanical wave packet for different times. We illustrated this decomposition explicitly for a coherent state. Its distribution being relatively steady, the characteristic function of a coherent state is peaked around $k \sim m$, $m \in \mathbb{Z}$. For periodic revivals, where $Z(t) = \chi(gt/\pi)$, this translates to $W(t)$ being peaked around $gt = m\pi$, as shown previously in Fig. 2. For quasi-periodic revivals, $Z(t)$ and $\chi(k)$ are not directly proportional, but the propagator $\mathcal{K}(k, t)$ defined in Eq. (14) maps $\chi(k)$ within one of its periods into one of the $W_m(t)$ shown in Fig. 3 (a). They are centered at the linearly-spaced intervals dictated by Eq. (24).

We wish to illustrate how to decompose other inversion profiles, and a cat state is a natural choice, given its relative simplicity. A cat state is usually defined as

$$|\xi\rangle \propto \frac{|\alpha\rangle + |\alpha e^{i\phi}\rangle}{\sqrt{2}}, \tag{28}$$

where $|\alpha\rangle$ is a coherent state with $\langle a^\dagger a\rangle = |\alpha|^2$. The symbol $\propto$ indicates that we have not normalized the state properly, though the missing proportionality factor approaches 1 for large α. We assume for simplicity that α is real.

The photon-number distribution of $|\xi\rangle$ is

$$P_n(\phi) \approx c_n^2 + c_n^2 \cos(n\phi), \tag{29}$$

where c_n^2 is the photon-number distribution of a coherent state, and we have assumed large α. The second term on the right-hand side of Eq. (29) oscillates with frequency dictated by ϕ. The oscillations are fastest when $\phi = \pi$, in which case P_n alternates between $2c_n^2$ (for even n) and 0 (for odd n). The characteristic function, being essentially a spectral decomposition of P_n, should be peaked around $k \sim 0$ (accounting for the steadier component of $\chi(k)$) and around $k \sim \frac{\phi}{2\pi}$ (accounting for the staggered component of $\chi(k)$). In fact, let $\chi_\alpha(k)$ be the characteristic function for $|\alpha\rangle$. Then, from Eq. (29), the characteristic function for $|\xi\rangle$ is

$$\chi(k, \phi) = \chi_\alpha(k) + \frac{1}{2}\chi_\alpha\left(k - \frac{\phi}{2\pi}\right) + \frac{1}{2}\chi_\alpha\left(k + \frac{\phi}{2\pi}\right). \tag{30}$$

In particular, for $\phi = \pi$, and already using the periodicity of $\chi(k, \phi)$,

$$\chi(k, \pi) = \chi_\alpha(k) + \chi_\alpha\left(k - \frac{1}{2}\right). \tag{31}$$

Due to the second term on the right-hand side of Eq. (31), this characteristic function features additional peaks around $k \sim m + 1/2$, $m \in \mathbb{Z}$.

Let us now look at the revivals of $|\xi\rangle$ and how they compare to revivals of $|\alpha\rangle$ in Fig. 5. Their initial collapses turn out to be, to a very good approximation, the same. At first, this is very unsettling: if we take the collapse as data for $W_0(t)$, a naive application of Eq. (27) will then yield (incorrectly) the distribution of a coherent state. On the other hand, the revivals of $|\xi\rangle$ seem to happen earlier. One may numerically check that using the first revival as data for $W_1(t)$ leads to unphysical (negative) probabilities.

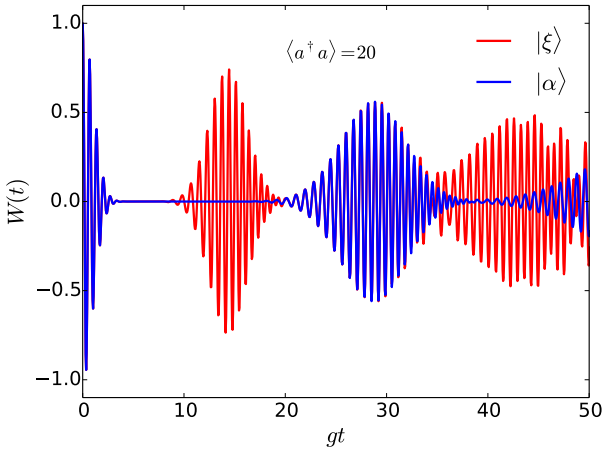

Figure 5. Revivals of a coherent state $|\alpha\rangle$ and a cat state $|\xi\rangle \propto |\alpha\rangle + |-\alpha\rangle$, with $\langle a^\dagger a\rangle = |\alpha|^2 = 20$. Since the characteristic function of these states is the same for low-frequencies, the collapse and some revivals coincide. However, the high-frequency components exclusive to $|\xi\rangle$ generate intermediate revivals arising from the oscillatory behaviour of the photon-number distribution of a cat state.

These puzzling features can be understood almost immediately in the framework of characteristic functions. To shed light on the matter, we first analyze periodic revivals, then argue that, as we deform $n \to \sqrt{n+1}$, the quasi-periodic revivals must remain qualitatively similar. When revivals are periodic, they are proportional to $\chi(k)$ itself. On the other hand, we expect $\chi(k)$, according to Eq. (31), to be peaked around m and $m-1/2$, with m an integer. Within a single period window, this corresponds to two peaks. As we now look at the JCM revivals, it is natural to still expect two peaks, albeit with modified shapes. This means that we should interpret the first collapse and the first revival of $|\xi\rangle$ seen in Fig. 5 as associated to a single period of $\chi(k)$ rather than separate objects.

This picture also explains why the initial collapses of both cat and coherent states overlap: the initial collapses being associated to the peak of $\chi(k)$ centered at $k \sim 0$, they are the same for states $|\alpha\rangle$ and $|\xi\rangle$ because the steadier components of the characteristic functions of both states are the same. On the other hand, the extra revivals of the cat state corresponds to the staggered components of $\chi(k, \pi)$, which are absent for a coherent state.

In conclusion, both the collapse and this early revival must be interpreted as $W_0(t)$. It is only when they are taken simultaneously into consideration that Eq. (27) yields the correct probabilities, as shown in Fig. 6. In Fig. 7 (a), we show the $W_0(t)$ used to retrieve the probabilities and the other $W_m(t)$ generated through Eq. (22). In Fig. 7 (b), we add them to show that we recover the full $W(t)$.

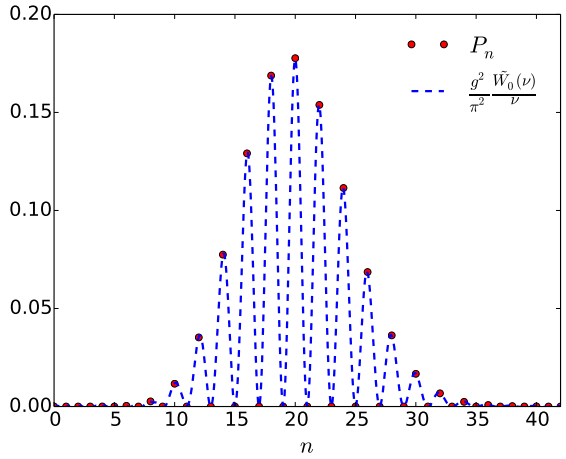

Figure 6. Comparison between the photon-number distribution of a cat state and Eq. (27) for $m = 0$. When collapse (and its symmetric extension for $t < 0$) and the first revival are accounted as $W_0(t)$, one retrieves the correct distribution.

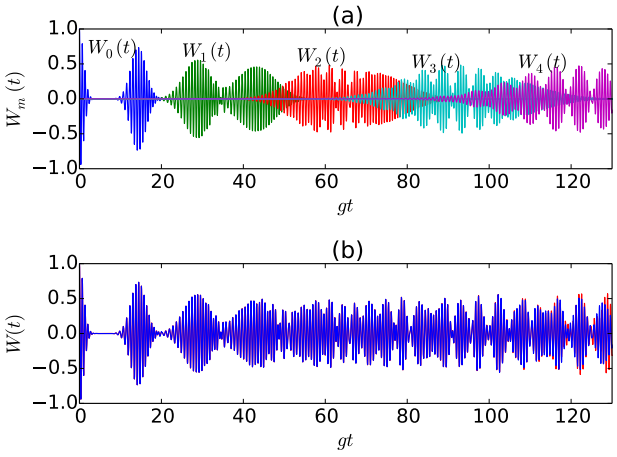

Figure 7. (a) Decomposition of the revivals of $|\xi\rangle$ as given by Eq. (28), with $\phi = \pi$, in terms of $W_m(t)$. Two consecutive revivals are part of the same $W_m(t)$. In the framework of characteristic functions, each correspond to the peaks of $\chi(k)$ centered around m and $m + 1/2$. (b) When we add the $W_m(t)$, we recover the full $W(t)$. The blue curve represents $\sum_{m=0}^{4} W_m(t)$ and the red curve represents the full $W(t)$. The agreement can be improved for even longer times by adding further $W_m(t)$.

A practical task is how to verify when revival is not a standalone $W_m(t)$. In our example we could simply compare the predicted probabilities, but we do not know the state behind the inversion profile in general. One approach to tackle this task is simply through trial and error: once a distribution has been predicted, $W(t)$ can be numerically calculated with Eq. (4) and compared with the experimental data for the inversion at later times. If comparison shows that the numerically calculated inversion is missing intermediate revivals, then the time range for $W_m(t)$ must be reselected, just as we did for a cat state.

Another check is that, since the additional revivals are not standalone $W_m(t)$, using just the additional revival in Eq. (27) will, in general, yield negative, hence non-physical, probabilities. They only make sense when added to the ones obtained through the collapse. Their combination should yield the correct probabilities.

V. OVERLAPPING $W_m(t)$

In the previous sections, we considered non-overlapping revivals so that $W_0(t)$ (or any other $W_m(t)$) can be obtained straightforwardly from $W(t)$, and Eq. (27) used to retrieve the field photon-number distribution. We now show that, with the decomposition presented in Sec. III, it is possible to circumvent this limitation and extract $W_0(t)$ even when revivals overlap. Therefore, our method allows photon-number distributions to be retrieved under fairly general conditions.

The key idea is that, if we sample $W(t)$ for a long enough time window $[-T, T]$, $W_0(t)$ will be completely captured, albeit tainted with tails of $W_1(t)$, $W_{-1}(t)$ and, more generally, every other $W_m(t)$. Here, we consider the simplest case where terms with $|m| > 1$ can be neglected, though the formalism is easy to acommodate otherwise. Considering the FFT of the limited window of $W(t)$ leads to the spectrum $\tilde{\mathcal{W}}(\nu)$:

$$\tilde{\mathcal{W}}(\nu) = \tilde{W}_0(\nu) + \int_{-\infty}^{\infty} d\nu' \, \frac{\sin\left[\pi(\nu-\nu')2T\right]}{\pi(\nu-\nu')} \left[\tilde{W}_1(\nu') + \tilde{W}_{-1}(\nu')\right], \tag{32}$$

The first term on the right-hand side of Eq. (32) is simply the spectrum of $W_0(t)$. However, $\tilde{\mathcal{W}}(\nu)$ is contamined by the second term, which arises from the convolution of $W_1(t)$ and $W_{-1}(t)$ with the window function located between $-T$ and T.

However, from Eq. (22), it may be shown that $\tilde{W}_1(\nu) + \tilde{W}_{-1}(\nu) = 2\tilde{W}_0(\nu)\cos\left[2\pi\left(\frac{\pi\nu}{g}\right)\right]^2 \tilde{W}_0(\nu)$, which means that Eq. (32) is, in fact, an integral equation for $\tilde{W}_0(\nu)$:

$$\tilde{\mathcal{W}}(\nu) = \tilde{W}_0(\nu) + \int_{-\infty}^{\infty} d\nu' \; S(\nu,\nu')\tilde{W}_0(\nu'), \tag{33}$$

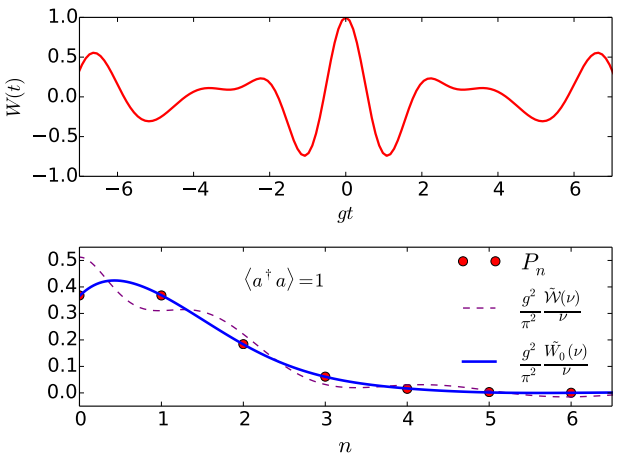

Figure 8. Inversion profile for a coherent state with $\langle a^\dagger a\rangle = 1$ and photon-number distribution retrieval through Eq. (33). For an average photon-number this low, the revivals cannot be clearly resolved anymore. We tentatively choose a time window running from -5 to 5. The Fourier transform of $W(t)$ under this window yields $\tilde{\mathcal{W}}(\nu)$, which we use to construct the (dashed) purple curve. This curve does not match the theoretical probability (represented by the red dots) because it is contaminated by the spectra of $W_1(t)$ and $W_{-1}(t)$. We have used Eq. (33) to solve for $\tilde{W}_0(\nu)$, which corresponds to the blue curve, yielding the correct probabilities.

where

$$S(\nu,\nu') = 2\cos\left[2\pi\left(\frac{\pi\nu'}{g}\right)\right]^2 \frac{\sin\left[\pi(\nu-\nu')2T\right]}{\pi(\nu-\nu')}. \tag{34}$$

This equation has the form of a Fredholm equation of the second kind, and can be solved numerically for $\tilde{W}_0(\nu)$, given the observed spectrum $\tilde{\mathcal{W}}(\nu)$ [55]. We consider the retrieval of $\tilde{W}_0(\nu)$, and the photon-number distribution through Eq. (27), for a coherent state with $n = 1$, for which revivals cannot be resolved. The results are presented in Fig. 8. Eq. (33) lays the foundation for our approach. A more detailed exposition of this technique will be presented in a later work.

VI. CONCLUSIONS

In this work, we exploited the characteristic function periodicity to split the inversion into a superposition of packets centered at different times. When the inversion oscillation frequencies are commensurable, the packets are perfect replicas of one another, and each one represents a single revival. In the case of the JCM, for which frequencies are incommensurable, the inversion $W(t)$ can still be split exactly into a set of packets $W_m(t)$. Knowledge of a single $W_m(t)$ determines every other $W_m(t)$, but they are now imperfect replicas, experiencing dispersion akin to that of free particles in quantum dynamics.

Once dispersion is accounted for, however, they become the same. Hence, it is also possible to retrieve the photon-number distribution underlying the revivals through just a single $W_m(t)$. When the $W_m(t)$ do not overlap, each of them can be identified with a single revival of $W(t)$.

We have illustrated the decomposition and also the distribution retrieval for a coherent state and a cat state. For a coherent state, the retrieval is straightforward. We have also shown how to generate all the subsequent $W_m(t)$ once $W_0(t)$ has been determined. As expected, adding them up yields the full population inversion. This formalism holds for any state (not just coherent states), but there may be caveats to consider. For example, for a cat state, care must be taking in identifying $W_0(t)$. In this case, the oscillating distribution leads to additional revivals. We have learned that the additional revivals must not be thought of as standalone revivals: they are a signature of the high k components of $\chi(k)$ and must be considered with the revivals arising from the low k components of $\chi(k)$ as part of a single $W_m(t)$ in order for probabilities to be correctly retrieved.

The characteristic function approach provides us with a new way of interpreting the inversion, but photon-number distribution retrieval methods through single revivals have been known for a while [47]. To highlight the practical advantages of our method, we have at last considered the case where revivals cannot be resolved anymore. We have outlined how to retrieve $W_m(t)$ under more general assumptions, and considered a coherent state with average photon-number of 1 as an example. By casting aside the limitation imposed by non-overlapping revivals, this work has set the stage for a new tomographic approach, which will investigate thoroughly in an upcoming work. Other interesting extensions of this work would be applying the formalism for other atomic properties, such as the atomic dipole. It would also be worth looking at how different profiles of $\chi(k)$ lead to different shapes of $W_m(t)$ by further investigating the propagator connecting these objects.

ACKNOWLEDGMENTS

The authors would like to thank D. Schmid, K. Marshall, J. Cresswell, N. Quesada and E. Tham for helpful discussions. This work was supported by NSERC.

[1] J. F. Clauser, Phys. Rev. D **9**, 853 (1974).
[2] P. Grangier, G. Roger, and A. Aspect, EPL **1**, 173 (1986).
[3] C. K. Hong, Z. Y. Ou, and L. Mandel, Physical Review Letters (1987).
[4] J. J. Thorn, M. S. Neel, V. W. Donato, G. S. Bergreen, R. E. Davies, and M. Beck, American Journal of Physics **72**, 1210 (2004).
[5] L.-A. Wu, H. J. Kimble, J. L. Hall, and H. Wu, Physical Review Letters **57**, 2520 (1986).
[6] R. E. Slusher, L. W. Hollberg, B. Yurke, J. C. Mertz, and J. F. Valley, Physical Review Letters **55**, 2409 (1985).
[7] A. Ourjoumtsev, H. Jeong, R. Tualle-Brouri, and P. Grangier, Nature **448**, 784 (2007).
[8] M. Hofheinz, E. M. Weig, M. Ansmann, R. C. Bialczak, E. Lucero, M. Neeley, A. D. O'Connell, H. Wang, J. M. Martinis, and A. N. Cleland, Nature **454**, 310 (2008).
[9] M. Hofheinz, H. Wang, M. Ansmann, R. C. Bialczak, E. Lucero, M. Neeley, A. D. O'Connell, D. Sank, J. Wenner, J. M. Martinis, and A. N. Cleland, Nature **459**, 546 (2009).
[10] D. Meschede, H. Walther, and G. Müller, Physical Review Letters **54**, 551 (1985).
[11] H. Walther, Phys. Scr. **1988**, 165 (1988).
[12] S. Horoche and D. Kleppner, Phys Today (1989).
[13] H. Walther, B. T. H. Varcoe, B.-G. Englert, and T. Becker, Rep. Prog. Phys. **69**, 1325 (2006).
[14] M. Brune, E. Hagley, J. Dreyer, X. Maitre, A. Maali, C. Wunderlich, J. M. Raimond, and S. Haroche, Physical Review Letters **77**, 4887 (1996).
[15] E. Hagley, X. Maitre, G. Nogues, C. Wunderlich, M. Brune, J. M. Raimond, and S. Haroche, Physical Review Letters **79**, 1 (1997).
[16] S. Brattke, B. T. H. Varcoe, and H. Walther, Physical Review Letters **86**, 3534 (2001).
[17] I. I. Rabi, Phys. Rev. **49**, 324 (1936).
[18] I. I. Rabi, Phys. Rev. **51**, 652 (1937).
[19] D. Braak, Physical Review Letters **107**, 100401 (2011).
[20] E. T. Jaynes and F. W. Cummings, Proceedings of the IEEE **51**, 89 (1963).
[21] B. W. Shore and P. L. Knight, Journal of Modern Optics **40**, 1195 (1993).
[22] J. H. Eberly, N. B. Narozhny, and J. J. Sanchez-Mondragon, Physical Review Letters **44**, 1323 (1980).
[23] M. Brune, F. Schmidt-Kaler, A. Maali, J. Dreyer, E. Hagley, J. M. Raimond, and S. Haroche, Physical Review Letters **76**, 1800 (1996).
[24] J. M. Fink, M. Göppl, M. Baur, R. Bianchetti, P. J. Leek, A. Blais, and A. Wallraff, Nature **454**, 315 (2008).
[25] N. B. Narozhny, J. J. Sanchez-Mondragon, and J. H. Eberly, Phys. Rev. A **23**, 236 (1981).
[26] P. Knight and P. Radmore, Phys. Rev. A **26**, 676 (1982).
[27] R. R. Puri and G. S. Agarwal, Phys. Rev. A **33**, 3610 (1986).
[28] S. J. D. Phoenix and P. L. Knight, Annals of Physics **186**, 381 (1988).
[29] P. F. Góra and C. Jedrzejek, Phys. Rev. A **49**, 3046 (1994).
[30] D. Jonathan, K. Furuya, and A. Vidiella-Barranco, Journal of Modern Optics **46**, 1697 (1999).
[31] U. Leonhardt and H. Paul, Progress in Quantum Electronics **19**, 89 (1995).
[32] S. Weigert, in *Compendium of Quantum Physics* (Springer Berlin Heidelberg, Berlin, Heidelberg, 2009) pp. 609–611.
[33] V. Bužek, G. Adam, and G. Drobný, Phys. Rev. A **54**, 804 (1996).
[34] D. F. V. James, P. G. Kwiat, W. J. Munro, and A. G.

White, Phys. Rev. A **64**, 052312 (2001).
[35] D. I. Schuster, A. A. Houck, J. A. Schreier, A. Wallraff, J. M. Gambetta, A. Blais, L. Frunzio, J. Majer, B. Johnson, M. H. Devoret, S. M. Girvin, and R. J. Schoelkopf, Nature **445**, 515 (2007).
[36] C. Guerlin, J. Bernu, S. Deleglise, C. Sayrin, S. Gleyzes, S. Kuhr, M. Brune, J.-M. Raimond, and S. Haroche, Nature **448**, 889 (2007).
[37] J. E. Moyal, Cambridge Philos. Soc. Math. Proc. **45**, 99 (1949).
[38] K. E. Cahill and R. J. Glauber, Phys. Rev. **177**, 1882 (1969).
[39] E. Wigner, Phys. Rev. **40**, 0749 (1932).
[40] K. Vogel and H. Risken, Phys. Rev. A **40**, 2847 (1989).
[41] D. T. Smithey, M. Beck, M. G. Raymer, and A. Faridani, Physical Review Letters **70**, 1244 (1993).
[42] A. I. Lvovsky and M. G. Raymer, Rev. Mod. Phys. **81**, 299 (2009).
[43] G. M. DAriano, C. Macchiavello, and M. G. A. Paris, Phys. Rev. A **50**, 4298 (1994).
[44] G. M. DAriano, U. Leonhardt, and H. Paul, Phys. Rev. A **52**, R1801 (1995).
[45] S. Wallentowitz and W. Vogel, Phys. Rev. A **53**, 4528 (1996).
[46] T. Opatrný and D. G. Welsch, Phys. Rev. A **55**, 1462 (1997).
[47] M. Fleischhauer and W. P. Schleich, Phys. Rev. A **47**, 4258 (1993).
[48] P. J. Bardroff, E. Mayr, and W. P. Schleich, Phys. Rev. A **51**, 4963 (1995).
[49] C. T. Bodendorf, G. Antesberger, M. S. Kim, and H. Walther, Phys. Rev. A **57**, 1371 (1998).
[50] L. G. Lutterbach and L. Davidovich, Physical Review Letters **78**, 2547 (1997).
[51] E. Lukacs, *Characteristic functions; 2nd ed.* (Griffin, London, 1970).
[52] B. Buck and C. V. Sukumar, Physics Letters A **81**, 132 (1981).
[53] P. L. Knight, Phys. Scr. **1986**, 51 (1986).
[54] S. J. D. Phoenix and P. L. Knight, J. Opt. Soc. Am. B, JOSAB **7**, 116 (1990).
[55] W. H. Press, S. A. Teukolsky, W. T. Vetterling, and B. P. Flannery, *Numerical Recipes in C: The Art of Scientific Computing* (Cambridge University Press, 1992).
[56] H. I. Yoo and J. H. Eberly, Physics Reports **118**, 239 (1985).